Hindawi
Mathematical Problems in Engineering
Volume 2017, Article ID 9452920, 12 pages
https://doi.org/10.1155/2017/9452920

Research Article

Safety-Guaranteed Trajectory Tracking Control for the Underactuated Hovercraft with State and Input Constraints

Mingyu Fu, Shuang Gao, and Chenglong Wang

College of Automation, Harbin Engineering University, Harbin 150001, China

Correspondence should be addressed to Shuang Gao; gaussian@hrbeu.edu.cn

Received 16 May 2017; Revised 14 August 2017; Accepted 24 September 2017; Published 25 October 2017

Academic Editor: Rafael Morales

Copyright © 2017 Mingyu Fu et al. This is an open access article distributed under the Creative Commons Attribution License, which permits unrestricted use, distribution, and reproduction in any medium, provided the original work is properly cited.

This paper develops a safety-guaranteed trajectory tracking controller for hovercraft by using a safety-guaranteed auxiliary dynamic system, an integral sliding mode control, and an adaptive neural network method. The safety-guaranteed auxiliary dynamic system is designed to implement system state and input constraints. By considering the relationship of velocity and resistance hump, the velocity of hovercraft is constrained to eliminate the effect of resistance hump and obtain better stability. And the safety limit of drift angle is well performed to guarantee the light safe maneuvers of hovercraft tracking with high velocities. In view of the natural capabilities of actuators, the control input is constrained. High nonlinearity and model uncertainties of hovercraft are approximated by employing adaptive radical basis function neural networks. The proposed controller guarantees the boundedness of all the closed-loop signals. Specifically, the tracking errors are uniformly ultimately bounded. Numerical simulations are implemented to demonstrate the efficacy of the designed controller.

1. Introduction

A hovercraft (Figure 1) is supported totally by its air cushion, with a flexible skirt system around its periphery to seal the cushion air [1]. The hovercraft is able to run at high speed over shallow water, rapids, ice, and swamp where no other craft can go. These "special abilities" have attracted many military and civil users with particular mission requirements. The study about the safety-guaranteed trajectory tracking control of underactuated hovercraft moving with high velocities is meaningful and challenging to reduce the burden of pilot.

From a detailed review of the available literatures about the trajectory tracking control of hovercraft [2–8], only position errors were considered and the velocities of hovercraft were not controlled. However, the velocity is related to the resistance hump of hovercraft. From [9], the resistance hump occurs in the vicinity of Froude number $F_r = 1$ which can be calculated by $F_r = V/\sqrt{gl_c}$, where V is the velocity of hovercraft and l_c is the cushion length. From [10], two resistance humps (mainly caused by wave-making drag) are encountered for hovercraft during the acceleration process. It is shown in [1] that the resistance hump will be crossed as F_r increases and the craft will travel with better course stability and transverse stability. Hence, the velocity of hovercraft needs to be large enough, corresponding to large F_r, to avoid the resistance hump and hold the better stability.

Moreover, drift angle plays a key role in the high-speed moving process of hovercraft [11, 12]. If the drift angle exceeds the angle of drift which corresponds to the maximum of hydrodynamic forces, the behavior of hovercraft will be nonstable [13]. The dangers caused by the drift angle include stern kickoff, plough-in, and great heeling [11]. Hence, safety limit of drift angle must be strictly obeyed in the high-speed tracking process to ensure safe maneuvers of hovercraft [12]. For instance, safety limit of a hovercraft shows if speed exceeds 40 knots, turning is not allowed; if speed is in the range of 25 knots~35 knots, drift angle needs to be within the limits of 7.5°~2°.

Besides, from a practical viewpoint, the control input is restrained to prevent the actuators from going beyond their natural capabilities [14, 15]. And radical basis function neural

Figure 1: A 3D model of hovercraft. Photo is from the international cooperation project described in Acknowledgments.

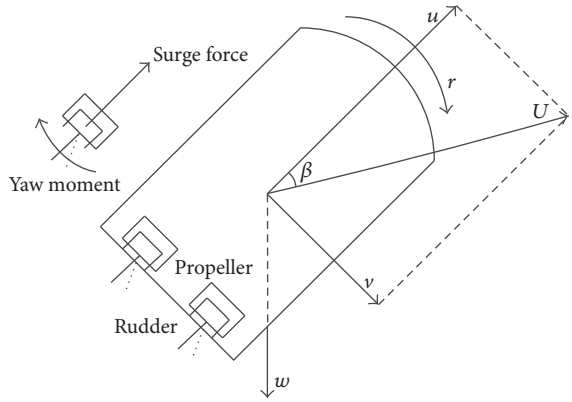

Figure 2: Diagram of underactuated hovercraft.

networks (RBFNNs) are used to stabilize complex nonlinear dynamic systems and deal with model uncertainties [16–18].

The contributions of this paper are as follows:

(i) The velocity of hovercraft is controlled within a reasonable range to avoid the effect of resistance hump and keep better stability.

(ii) The safety limit of drift angle is obeyed to get light safe maneuvers of hovercraft moving with high velocities.

(iii) The control input is constrained to handle input saturation.

This paper is organized as follows. Section 2 establishes a nonlinear model of underactuated hovercraft and the transformation of it. Section 3 proposes a safety-guaranteed auxiliary dynamic system for state and input constraints. Moreover, the controller is designed and analyzed in this section. Numerical simulation results are shown in Section 4, and the conclusion is discussed in Section 5.

2. Problem Formulation

2.1. Hovercraft Model Description. In general, only air propellers and rudders are available for hovercraft as shown in Figure 2. It means only the surge and yaw can be regulated directly, but without any actuators for their sway motion [19, 20].

The nonlinear model of hovercraft is obtained by neglecting the roll and pitch motions.

$$[\dot{x}\ \ \dot{y}\ \ \dot{z}\ \ \dot{\psi}]^T = S(\psi)[u\ \ v\ \ w\ \ r]^T,$$

$$\begin{bmatrix} \dot{u} \\ \dot{v} \\ \dot{w} \\ \dot{r} \end{bmatrix} = \begin{bmatrix} vr \\ -ur \\ 0 \\ 0 \end{bmatrix} + M \begin{bmatrix} R_u + \tau_u \\ R_v \\ R_w - p_c S_c \\ R_r + \tau_r \end{bmatrix}, \tag{1}$$

where

$$S(\psi) = \begin{bmatrix} \cos\psi & -\sin\psi & 0 & 0 \\ \sin\psi & \cos\psi & 0 & 0 \\ 0 & 0 & 1 & 0 \\ 0 & 0 & 0 & 1 \end{bmatrix},$$

$$M = \begin{bmatrix} \frac{1}{m} & 0 & 0 & 0 \\ 0 & \frac{1}{m} & 0 & 0 \\ 0 & 0 & \frac{1}{m} & 0 \\ 0 & 0 & 0 & \frac{1}{J_z} \end{bmatrix}; \tag{2}$$

the signals u, v, and w represent the surge, sway, and heave velocities, r is the turn rate, x, y, and z denote the position of hovercraft's mass center in the earth fixed frame, ψ describes yaw angle, m and J_z are hovercraft's mass and moments of inertia, τ_u and τ_r are the control inputs which are provided by the actuators, p_c is the average cushion pressure, S_c is the cushion area, and $[R_u\ \ R_v\ \ R_w\ \ R_r]^T$ are the total drags written as

$$R_m = \rho_a \overline{V}_a Q,$$

$$R_{\mathrm{wm}} = \frac{C_{\mathrm{wm}} p_c^2 B_c}{\rho_w g},$$

$$R_{\mathrm{sk}} = 0.5\rho_w V_a^2 C_{\mathrm{sk}} \left(\frac{h}{l_{\mathrm{sk}}}\right)^{-0.34} l_{\mathrm{sk}} S_c^{0.5} + \left(2.8167 \left(\frac{p_c}{l_c}\right)^{-0.259} - 1\right) R_{\mathrm{wm}},$$

$$\begin{aligned} R_u &= R_{ua} + R_{um} + R_{u\mathrm{wm}} + R_{u\mathrm{sk}} \\ &= -0.5\rho_a V_a^2 C_{ua} S_{\mathrm{PP}} - R_m \cos\beta - R_{\mathrm{wm}} \cos\beta \\ &\quad - R_{\mathrm{sk}} \cos\beta, \end{aligned}$$

$$\begin{aligned} R_v &= R_{va} + R_{vm} + R_{v\mathrm{wm}} + R_{v\mathrm{sk}} \\ &= -0.5\rho_a V_a^2 C_{va} S_{\mathrm{LP}} - R_m \sin\beta - R_{\mathrm{wm}} \sin\beta \\ &\quad - R_{\mathrm{sk}} \sin\beta, \end{aligned}$$

$$\begin{aligned} R_w &= R_{wa} + R_{w\mathrm{wm}} + G \\ &= -0.5\rho_a V_a^2 C_{wa} S_{\mathrm{HP}} - \rho_a w Q + G, \end{aligned}$$

$$\begin{aligned} R_r &= R_{ra} + R_{rm} + R_{r\mathrm{wm}} + R_{r\mathrm{sk}} \\ &= -0.5\rho_a V_a^2 C_{ra} S_{\mathrm{HP}} H_{\mathrm{hov}} - R_{va} \times x_a + R_{ua} \times y_a \\ &\quad - R_{vm} x_m + R_{um} y_m - R_{v\mathrm{wm}} x_{\mathrm{wm}} + R_{u\mathrm{wm}} y_{\mathrm{wm}} \\ &\quad - R_{v\mathrm{sk}} x_{\mathrm{sk}} + R_{u\mathrm{sk}} y_{\mathrm{sk}}, \end{aligned} \tag{3}$$

where the drag's suffix a is the aerodynamic profile drag, wm is the wave-making drag, m is the air momentum drag, sk is the skirt drag, C_{ua}, C_{va}, C_{pa}, C_{ra}, C_{wm}, and C_{sk} are the drag coefficients, B_c is the cushion beam, l_c is the cushion length, G is the weight, S_{PP}, S_{LP}, and S_{HP} are the positive, lateral, and horizontal projection areas, β is the drift angle, Q is the fan flow rate of cushion fan, h is the distance between baffle and the bottom of skirt's finger, l_{sk} is the total peripheral length of the skirts, H_{hov} is the height of hovercraft, ρ_a and ρ_w are air and water density, and (x_a, y_a), (x_m, y_m), $(x_{\mathrm{wm}}, y_{\mathrm{wm}})$, and $(x_{\mathrm{sk}}, y_{\mathrm{sk}})$ are the coordinates of force's acting points.

$\overline{V}_a$ and V_a in (3) can be obtained by

$$\begin{aligned} &\overline{V}_a \\ &= \sqrt{\left[u + V_w \cos\left(\beta_w - \psi\right)\right]^2 + \left[v + V_w \sin\left(\beta_w - \psi\right)\right]^2}, \\ &V_a = \sqrt{\overline{V}_a^2 + w^2}, \end{aligned} \tag{4}$$

in which V_w and β_w are absolute wind speed and direction. More details can be found in [1, 9, 21].

Remark 1. When a hovercraft is moving on a calm water surface, cushion pressure p_c varies within a narrow range and the heave motion is stable. This paper is the research about the horizontal motion of the hovercraft. Hence, the heave motion is not discussed and the cushion pressure p_c is assumed to be a constant.

From Figure 2, we have

$$v = u \tan\left(\beta\right). \tag{5}$$

In order to make β be the system state and more convenient for the constraint and control of β, an improved model is derived from (1) and (5); that is,

$$\begin{aligned} \begin{bmatrix} \dot{x} & \dot{y} & \dot{z} & \dot{\psi} \end{bmatrix}^T &= S\left(\psi\right) \begin{bmatrix} u & u\tan\beta & w & r \end{bmatrix}^T, \\ \begin{bmatrix} \dot{u} \\ \dot{\beta} \\ \dot{w} \\ \dot{r} \end{bmatrix} &= \begin{bmatrix} ur\tan\beta \\ -\dfrac{\dot{u}\sin\left(2\beta\right)}{2u} - r\cos^2\beta \\ 0 \\ 0 \end{bmatrix} \\ &\quad + M \begin{bmatrix} R_u + \tau_u \\ R_v \dfrac{\cos^2\beta}{u} \\ R_w - p_c S_c \\ R_r + \tau_r \end{bmatrix}. \end{aligned} \tag{6}$$

2.2. State and Input Constraints. Saturation nonlinearities of actuators can be described by

$$\tau_\varpi = \mathrm{sat}\left(\tau_{\varpi c}, \tau_{\varpi \mathrm{cmax}}, \tau_{\varpi \mathrm{cmin}}\right), \quad \varpi = u, r, \tag{7}$$

where $\tau_{\varpi \mathrm{cmax}}$ and $\tau_{\varpi \mathrm{cmin}}$ are the maximum and minimum limitations of actuators, $\tau_{\varpi c}$ are the designed control laws, and sat$(\cdot)$ is a generalized saturation function with the following form:

$$\mathrm{sat}\left(\alpha, \alpha_M, \alpha_m\right) = \begin{cases} \alpha_M, & \text{if } \alpha > \alpha_M, \\ \alpha, & \text{if } \alpha_m \le \alpha \le \alpha_M, \\ \alpha_m, & \text{if } \alpha < \alpha_m. \end{cases} \tag{8}$$

Assumption 2. All position, orientation, velocity, and acceleration values of hovercraft are available for feedback.

Safety limit of β and hump speed of hovercraft need to be obtained from model and real ship tests [11, 12]. In this paper, they are assumed to be known and available for the state constraint. Then the safe constraints of system state are defined as

$$\begin{aligned} u_{\mathrm{min}} \le u \le u_{\mathrm{max}}, \\ \beta_{\mathrm{min}} \le \beta \le \beta_{\mathrm{max}}. \end{aligned} \tag{9}$$

3. Controller Design

3.1. Safety-Guaranteed Auxiliary Dynamic System

Proposition 3. *A constraint error function is designed as follows:*

$$\begin{aligned} \Delta\kappa = {} & k_{w1}\left(\mathrm{sat}\left(x, x_{max}, x_{min}\right) - x\right) \\ & + k_{w2}\left(\mathrm{sat}\left(u_c, u_{c\,max}, u_{c\,min}\right) - u_c\right), \end{aligned} \tag{10}$$

where $k_{w1} > 0$, $k_{w2} > 0$, x is the system state, and u_c is the designed control input.

Then an auxiliary dynamic system is designed by

$$\dot{\xi} = \begin{cases} -k_{\xi 1}\xi - \dfrac{\vartheta\left(\cdot\right) + k_{\xi 2}\Delta\kappa^2}{\left\|\xi\right\|^2}\xi + \Delta\kappa, & \left\|\xi\right\| \ge \sigma, \\ deadzone\left(\Delta\kappa, \overline{\sigma}\right), & \left\|\xi\right\| < \sigma, \end{cases} \tag{11}$$

where ξ is the state of the auxiliary dynamic system, $k_{\xi 1}$, $k_{\xi 2}$ are positive constants, σ, $\overline{\sigma}$ are positive small design constants, $\vartheta(\cdot)$ can be derived from the stability analysis, and deadzone$(\Delta\kappa, \overline{\sigma})$ is a dead zone function given by

$$deadzone\left(\Delta\kappa, \overline{\sigma}\right) = \begin{cases} \Delta\kappa, & if\ \Delta\kappa > \overline{\sigma}, \\ 0, & if\ -\overline{\sigma} < \Delta\kappa \le \overline{\sigma}, \\ \Delta\kappa, & if\ \Delta\kappa \le \overline{\sigma}. \end{cases} \tag{12}$$

3.2. Design of the Desired States. Desired reference trajectory is generated by a virtual ship described in the following form:

$$\begin{bmatrix} \dot{x}_d \\ \dot{y}_d \\ \dot{\psi}_d \end{bmatrix} = \begin{bmatrix} \cos\psi_d & -\sin\psi_d & 0 \\ \sin\psi_d & \cos\psi_d & 0 \\ 0 & 0 & 1 \end{bmatrix} \begin{bmatrix} u_{d\mathrm{set}} \\ v_{d\mathrm{set}} \\ r_{d\mathrm{set}} \end{bmatrix}. \tag{13}$$

Then the trajectory tracking errors are defined as

$$(x_e, y_e) = (x - x_d, y - y_d). \tag{14}$$

For the position tracking, the desired states are designed by

$$\begin{aligned} u_d &= (\dot{x}_d - k_x |x_e| \operatorname{sign}(x_e)) \cos\psi + \left(\dot{y}_d - k_y |y_e| \right. \\ &\quad \left. \cdot \operatorname{sign}(y_e)\right) \sin\psi, \\ \beta_d &= \arctan\left(-\frac{\dot{x}_d - k_x |x_e| \operatorname{sign}(x_e)}{u_d} \sin\psi \right. \\ &\quad \left. + \frac{\dot{y}_d - k_y |y_e| \operatorname{sign}(y_e)}{u_d} \cos\psi \right), \end{aligned} \tag{15}$$

where $k_x > 0$ and $k_y > 0$ are control gains.

Remark 4. To guarantee the traceability of the reference trajectory under state constraints, the desired reference trajectory needs to satisfy the following conditions:

(C1) η_d, $\dot{\eta}_d$, and $\ddot{\eta}_d$ are all bounded, in which $\eta_d = \{x_d, y_d, \psi_d\}$.

(C2) There exists $T_r > 0$ such that, for all $t > T_r$,

$$\begin{aligned} u_{\min} < u_d < u_{\max}, \\ \beta_{\min} < \beta_d < \beta_{\max}. \end{aligned} \tag{16}$$

3.3. Controller Design. State tracking errors are defined as

$$\begin{aligned} e_u &= u - u_d, \\ e_\beta &= \beta - \beta_d. \end{aligned} \tag{17}$$

Then two integral sliding mode manifolds are given by

$$\begin{aligned} s_u &= e_u + \lambda_1 \int_0^t e_u \, d\tau, \\ s_r &= \dot{e}_\beta + \lambda_2 e_\beta + \lambda_3 \int_0^t e_\beta \, d\tau, \end{aligned} \tag{18}$$

where λ_1, λ_2, and λ_3 are positive constants.

Using (6), (17), and (18), the time derivatives of s_u and s_r are expressed as

$$\begin{aligned} \dot{s}_u &= \dot{e}_u + \lambda_1 e_u \\ &= f_u(\mathbf{x}_u) + M_u \tau_u + M_u R_u - \dot{u}_d + \lambda_1 e_u, \end{aligned} \tag{19}$$

$$\begin{aligned} \dot{s}_r &= \ddot{e}_\beta + \lambda_2 \dot{e}_\beta + \lambda_3 e_\beta \\ &= f_r(\mathbf{x}_r) + M_r \tau_r + D_{rw} - \ddot{\beta}_d + \lambda_2 \dot{e}_\beta + \lambda_3 e_\beta, \end{aligned} \tag{20}$$

where

$$\begin{aligned} f_u(\mathbf{x}_u) &= ur \tan\beta, \quad \mathbf{x}_u = [u, \beta, r]^T, \\ f_r(\mathbf{x}_r) &= -\frac{\ddot{u}u - \dot{u}^2}{2u^2} \sin(2\beta) - \frac{\dot{u}\dot{\beta}}{u} \cos(2\beta) \\ &\quad + \dot{\beta} r \sin(2\beta), \quad \mathbf{x}_r = \left[u, \dot{u}, \ddot{u}, r, \beta, \dot{\beta}\right]^T, \\ M_u &= \frac{1}{m}, \\ M_r &= -\frac{\cos^2\beta}{J_z}, \\ D_{rw} &= -\frac{\dot{\beta} R_v \sin(2\beta)}{um} + \frac{u\dot{R}_v - \dot{u}R_v}{u^2 m} \cos^2\beta \\ &\quad - \frac{R_r \cos^2\beta}{J_z}. \end{aligned} \tag{21}$$

To deal with high nonlinearity and model uncertainties, $f_u(\mathbf{x}_u)$ and $f_r(\mathbf{x}_r)$ are approximated by RBFNNs.

$$f_\varpi(\mathbf{x}_\varpi) = \mathbf{W}_\varpi^{*T} \mathbf{H}_\varpi(\mathbf{x}_\varpi) + \varepsilon_\varpi, \quad \varpi = u, r, \tag{22}$$

where $\mathbf{x}_\varpi \in R^I$ is the input vector and $\mathbf{W}_\varpi^* \in R^n$ is the ideal weight vector. $\mathbf{H}_\varpi(\mathbf{x}_\varpi) : R^I \to R^n$ is the basis function vector with element $h_{i\varpi}(\mathbf{x}_\varpi)$ shown as follows:

$$h_{i\varpi}(\mathbf{x}_\varpi) = \exp\left(-\frac{\|\mathbf{x}_\varpi - \boldsymbol{\mu}_{i\varpi}\|}{2\sigma_i^2} \right), \tag{23}$$

where $\boldsymbol{\mu}_{i\varpi}$ is the center of the receptive field and σ_i is the width of the Gaussian function. The approximation error ε_ϖ satisfies $|\varepsilon_\varpi| \le \varepsilon_N$.

Using (10) and (11), constraint error functions are designed as follows:

$$\begin{aligned} \Delta\kappa_u &= k_{wu1} (\operatorname{sat}(u, u_{\max}, u_{\min}) - u) \\ &\quad + k_{wu2} (\operatorname{sat}(\tau_{uc}, \tau_{uc\max}, \tau_{uc\min}) - \tau_{uc}), \\ \Delta\kappa_r &= k_{wr1} (\operatorname{sat}(\beta, \beta_{\max}, \beta_{\min}) - \beta) \\ &\quad + k_{wr2} (\operatorname{sat}(\tau_{rc}, \tau_{rc\max}, \tau_{rc\min}) - \tau_{rc}), \end{aligned} \tag{24}$$

where $k_{wu1} > 0$, $k_{wu2} > 0$, $k_{wr1} > 0$, and $k_{wr2} > 0$.

Then the auxiliary dynamic system is designed as

$$\begin{aligned} &\dot{\xi}_\varpi \\ &= \begin{cases} \left(-k_{\xi\varpi 1} \xi_\varpi - \dfrac{\vartheta_\varpi(\cdot) + k_{\xi\varpi 2} \Delta\kappa_\varpi^2}{\|\xi_\varpi\|^2} \xi_\varpi + \Delta\kappa_\varpi \right), & \|\xi_\varpi\| \ge \sigma, \\ \operatorname{deadzone}(\Delta\kappa_\varpi, \overline{\sigma}), & \|\xi_\varpi\| < \sigma, \end{cases} \end{aligned} \tag{25}$$

where $\vartheta_\varpi(\cdot) = |M_\varpi s_\varpi| |\tau_\varpi - \tau_{\varpi c}|$ and $\varpi = u, r$.

Finally, the control laws are given by

$$\tau_{uc} = \frac{1}{M_u}\left(-k_1 s_u - \eta_1 \operatorname{sign}(s_u) + \dot{u}_d - \lambda_1 e_u - M_u R_u - \widehat{\mathbf{W}}_u^T \mathbf{H}_u(\mathbf{x}_u) - \varepsilon_N \operatorname{sign}(s_u) + k_{su}\xi_u\right), \tag{26}$$

$$\tau_{rc} = \frac{1}{M_r}\left(\ddot{\beta}_d - k_2 s_r - \eta_2 \operatorname{sign}(s_r) - \lambda_2 \dot{e}_\beta - D_{rw} - \lambda_3 e_\beta - \widehat{\mathbf{W}}_r^T \mathbf{H}_r(\mathbf{x}_r) - \varepsilon_N \operatorname{sign}(s_r) + k_{sr}\xi_r\right), \tag{27}$$

where k_1, k_2, η_1, η_2, k_{su}, and k_{sr} are positive constants, $\widehat{\mathbf{W}}_u = \widetilde{\mathbf{W}}_u + \mathbf{W}_u^*$, $\widehat{\mathbf{W}}_r = \widetilde{\mathbf{W}}_r + \mathbf{W}_r^*$, and D_{rw} is defined in (20).

And the adaptive laws are

$$\dot{\widehat{\mathbf{W}}}_\varpi = \gamma_\varpi s_\varpi \mathbf{H}_\varpi(\mathbf{x}_\varpi) \quad \varpi = u, r, \tag{28}$$

where γ_ϖ is the adaptive coefficient.

3.4. Stability Analysis

Theorem 5. *If the state tracking errors (17), the desired states (15), the auxiliary dynamic system (25), the surge control law τ_{uc} (26), the yaw control law τ_{rc} (27), and the adaptive laws (28) are applied to the hovercraft system represented by (6) and, for any bounded initial condition, the closed-loop control system signals s_u, s_r, ξ_u, ξ_r, e_u, e_β, x_e, y_e and $\widetilde{w}_{iu}$ and $\widetilde{w}_{ir}$, $i = 1, 2, \ldots, n$, are uniformly ultimately bounded (UUB). The position and desired state tracking errors can be made arbitrarily small by appropriately selecting design parameters. And the yaw motion will remain bounded.*

Proof. The following Lyapunov function is defined:

$$V = \frac{1}{2}s_u^2 + \frac{1}{2}s_r^2 + \frac{1}{2\gamma_u}\widetilde{\mathbf{W}}_u^T\widetilde{\mathbf{W}}_u + \frac{1}{2\gamma_r}\widetilde{\mathbf{W}}_r^T\widetilde{\mathbf{W}}_r + \frac{1}{2}\xi_u^2 + \frac{1}{2}\xi_r^2. \tag{29}$$

From (19), (20), and (29), $\dot{V}$ can be expressed as

$$\dot{V} = s_u\left(f_u(\mathbf{x}_u) + M_u\tau_u + M_u R_u - \dot{u}_d + \lambda_1 e_u\right) + s_r\left(f_r(\mathbf{x}_r) + M_r\tau_r + D_{rw} - \ddot{\beta}_d + \lambda_2\dot{e}_\beta + \lambda_3 e_\beta\right) + \frac{\widetilde{\mathbf{W}}_u^T\dot{\widehat{\mathbf{W}}}_u}{\gamma_u} + \frac{\widetilde{\mathbf{W}}_r^T\dot{\widehat{\mathbf{W}}}_r}{\gamma_r} + \xi_u\dot{\xi}_u + \xi_r\dot{\xi}_r. \tag{30}$$

By defining $\tau_\varpi = \Delta\tau_\varpi + \tau_{\varpi c}$ and $\varpi = u, r$ and using (22), (26), and (27), we have

$$\dot{V} = -k_1 s_u^2 - \eta_1|s_u| + s_u\left(-\widetilde{\mathbf{W}}_u^T\mathbf{H}_u(\mathbf{x}_u)\right) + M_u s_u\Delta\tau_u + k_{su}s_u\xi_u + \left(-\varepsilon_N|s_u| + \varepsilon_u s_u\right) - k_2 s_r^2 - \eta_2|s_r| + s_r\left(-\widetilde{\mathbf{W}}_r^T\mathbf{H}_r(\mathbf{x}_r)\right) + M_r s_r\Delta\tau_r + k_{sr}s_r\xi_r + \left(-\varepsilon_N|s_r| + \varepsilon_r s_r\right) + \frac{1}{\gamma_u}\widetilde{\mathbf{W}}_u^T\dot{\widehat{\mathbf{W}}}_u + \frac{1}{\gamma_r}\widetilde{\mathbf{W}}_r^T\dot{\widehat{\mathbf{W}}}_r + \xi_u\dot{\xi}_u + \xi_r\dot{\xi}_r. \tag{31}$$

By using $|\varepsilon_\varpi| \le \varepsilon_N$ and $\varpi = u, r$, (31) can be rewritten as

$$\dot{V} \le -k_1 s_u^2 - \eta_1|s_u| + s_u\left(-\widetilde{\mathbf{W}}_u^T\mathbf{H}_u(\mathbf{x}_u)\right) - k_2 s_r^2 - \eta_2|s_r| + s_r\left(-\widetilde{\mathbf{W}}_r^T\mathbf{H}_r(\mathbf{x}_r)\right) + M_u s_u\Delta\tau_u + k_{su}s_u\xi_u + M_r s_r\Delta\tau_r + k_{sr}s_r\xi_r + \frac{1}{\gamma_u}\widetilde{\mathbf{W}}_u^T\dot{\widehat{\mathbf{W}}}_u + \frac{1}{\gamma_r}\widetilde{\mathbf{W}}_r^T\dot{\widehat{\mathbf{W}}}_r + \xi_u\dot{\xi}_u + \xi_r\dot{\xi}_r. \tag{32}$$

Substituting adaptive laws (28) into it yields

$$\dot{V} \le -k_1 s_u^2 + M_u s_u\Delta\tau_u + k_{su}s_u\xi_u + \xi_u\dot{\xi}_u - k_2 s_r^2 + M_r s_r\Delta\tau_r + k_{sr}s_r\xi_r + \xi_r\dot{\xi}_r. \tag{33}$$

The process of stability analysis is, respectively, discussed in the following two cases.

Case 1. When $\|\xi_\varpi\| \ge \sigma$, in light of (25) and Young's inequality, we have

$$\begin{aligned}\xi_\varpi\dot{\xi}_\varpi &= \xi_\varpi\Delta\kappa_\varpi - k_{\xi\varpi 1}\xi_\varpi^2 - k_{\xi\varpi 2}\Delta\kappa_\varpi^2 - |M_\varpi s_\varpi|\,|\tau_\varpi - \tau_{\varpi c}| \\ &\le k_{\xi\varpi 2}\Delta\kappa_\varpi^2 + \frac{1}{4k_{\xi\varpi 2}}\xi_\varpi^2 - k_{\xi\varpi 1}\xi_\varpi^2 - k_{\xi\varpi 2}\Delta\kappa_\varpi^2 - |M_\varpi s_\varpi|\,|\tau_\varpi - \tau_{\varpi c}| \\ &= -\left(k_{\xi\varpi 1} - \frac{1}{4k_{\xi\varpi 2}}\right)\xi_\varpi^2 - |M_\varpi s_\varpi|\,|\tau_\varpi - \tau_{\varpi c}|.\end{aligned} \tag{34}$$

Substituting $\tau_\varpi = \Delta\tau_\varpi + \tau_{\varpi c}$ and (34) into (33) and using Young's inequality yield

$$\begin{aligned}\dot{V} &\le -k_1 s_u^2 + k_{su}s_u\xi_u - \left(k_{\xi u1} - \frac{1}{4k_{\xi u2}}\right)\xi_u^2 - k_2 s_r^2 + k_{sr}s_r\xi_r - \left(k_{\xi r1} - \frac{1}{4k_{\xi r2}}\right)\xi_r^2 \\ &\le -(k_1 - 0.5)s_u^2 - \left(k_{\xi u1} - \frac{1}{4k_{\xi u2}} - 0.5k_{su}^2\right)\xi_u^2 - (k_2 - 0.5)s_r^2 - \left(k_{\xi r1} - \frac{1}{4k_{\xi r2}} - 0.5k_{sr}^2\right)\xi_r^2 \\ &\quad - \frac{k_1\widetilde{\mathbf{W}}_u^T\widetilde{\mathbf{W}}_u}{\gamma_u} - \frac{k_2\widetilde{\mathbf{W}}_r^T\widetilde{\mathbf{W}}_r}{\gamma_r} + \frac{k_1\widetilde{\mathbf{W}}_u^T\widetilde{\mathbf{W}}_u}{\gamma_u} + \frac{k_2\widetilde{\mathbf{W}}_r^T\widetilde{\mathbf{W}}_r}{\gamma_r} \le -2\mu_1 V + \rho_1,\end{aligned} \tag{35}$$

where

$$\mu_1 = \min\left\{(k_1 - 0.5), \left(k_{\xi u1} - \frac{1}{4k_{\xi u2}} - 0.5k_{su}^2\right), (k_2 - 0.5), \left(k_{\xi r1} - \frac{1}{4k_{\xi r2}} - 0.5k_{sr}^2\right)\right\},$$
$$\rho_1 = \frac{k_1}{\gamma_u}\widetilde{\mathbf{W}}_u^T\widetilde{\mathbf{W}}_u + \frac{k_2}{\gamma_r}\widetilde{\mathbf{W}}_r^T\widetilde{\mathbf{W}}_r. \tag{36}$$

Case 2. When $\|\xi_\omega\| < \sigma$, in light of (25) and Young's inequality, we have

$$\xi_\omega\dot{\xi}_\omega = \xi_\omega \text{deadzone}\left(\Delta\kappa_\omega, \overline{\sigma}\right) \le 0.5\xi_\omega^2 + 0.5\Delta\kappa_\omega^2,$$
$$0.5k_{s\omega}^2\xi_\omega^2 = k_{s\omega}^2\xi_\omega^2 - 0.5k_{s\omega}^2\xi_\omega^2 \le -0.5k_{s\omega}^2\xi_\omega^2 + k_{s\omega}^2\sigma^2. \tag{37}$$

Substituting (37) into (33) and using Young's inequality yield

$$\begin{aligned}\dot{V} &\le -k_1 s_u^2 + M_u s_u\Delta\tau_u + k_{su}s_u\xi_u + 0.5\xi_u^2 + 0.5\Delta\kappa_u^2 \\ &\quad - k_2 s_r^2 + M_r s_r\Delta\tau_r + k_{sr}s_r\xi_r + 0.5\xi_r^2 + 0.5\Delta\kappa_r^2 \\ &\le -(k_1 - 1)s_u^2 - (k_2 - 1)s_r^2 + 0.5M_u^2\Delta\tau_u^2 \\ &\quad + 0.5M_r^2\Delta\tau_r^2 + 0.5k_{su}^2\xi_u^2 + 0.5k_{sr}^2\xi_r^2 + 0.5\xi_u^2 \\ &\quad + 0.5\Delta\kappa_u^2 + 0.5\xi_r^2 + 0.5\Delta\kappa_r^2 \\ &\le -(k_1 - 1)s_u^2 - (k_2 - 1)s_r^2 - 0.5\xi_u^2\left(k_{su}^2 - 1\right) \\ &\quad - 0.5\xi_r^2\left(k_{sr}^2 - 1\right) + 0.5M_u^2\Delta\tau_u^2 + 0.5M_r^2\Delta\tau_r^2 \\ &\quad + k_{su}^2\sigma^2 + k_{sr}^2\sigma^2 + 0.5\Delta\kappa_u^2 + 0.5\Delta\kappa_r^2 \\ &\le -2\mu_2 V + \rho_2,\end{aligned} \tag{38}$$

where

$$\mu_2 = \min\left\{(k_1 - 1), \left(0.5k_{su}^2 - 0.5\right), (k_2 - 1), \left(0.5k_{sr}^2 - 0.5\right)\right\},$$
$$\rho_2 = \frac{k_1}{\gamma_u}\widetilde{\mathbf{W}}_u^T\widetilde{\mathbf{W}}_u + \frac{k_2}{\gamma_r}\widetilde{\mathbf{W}}_r^T\widetilde{\mathbf{W}}_r + 0.5M_u^2\Delta\tau_u^2 + 0.5M_r^2\Delta\tau_r^2 + \left(k_{su}^2 + k_{sr}^2\right)\sigma^2 + \frac{\left(\Delta\kappa_u^2 + \Delta\kappa_r^2\right)}{2}. \tag{39}$$

Synthesizing (35) and (38), we have

$$\dot{V} \le -2\mu V + \rho, \tag{40}$$

where $\mu = \min\{\mu_1, \mu_2\}$ and $\rho = \max\{\rho_1, \rho_2\}$ with the design parameters k_1, k_2, k_{su}, k_{sr}, $k_{\xi u1}$, $k_{\xi u2}$, $k_{\xi r1}$, and $k_{\xi r2}$ satisfying

$$k_1 > 1,$$
$$k_2 > 1,$$
$$k_{su} > 1,$$
$$k_{sr} > 1,$$
$$k_{\xi u1} - \frac{1}{4k_{\xi u2}} - 0.5k_{su}^2 > 0,$$
$$k_{\xi r1} - \frac{1}{4k_{\xi r2}} - 0.5k_{sr}^2 > 0. \tag{41}$$

Solving (40), we have

$$0 \le V(t) \le \frac{\rho}{2\mu} + \left[V(0) - \frac{\rho}{2\mu}\right]e^{-2\mu t}. \tag{42}$$

It is obviously seen that $V(t)$ is UUB for all $V(0) \le B_0$ with B_0 being any positive constant. Therefore, in the light of (29), we know that s_u, s_r, ξ_u, ξ_r and $\widetilde{w}_{iu}$ and $\widetilde{w}_{ir}$, $i = 1, 2, \ldots, n$, are UUB for all $V(0) \le B_0$. It can be expressed as

$$\|\chi\| \le \sqrt{\frac{\rho}{\mu} + 2\left[V(0) - \frac{\rho}{2\mu}\right]e^{-2\mu t}}, \tag{43}$$

where $\chi = \{s_u, s_r, \xi_u, \xi_r, \widetilde{w}_{iu}, \widetilde{w}_{ir}\}$.

It implies that there exists $T > 0$ such that, for all $t > T$,

$$\|\chi\| \le \sqrt{\frac{\rho}{\mu}}, \tag{44}$$

where $\sqrt{\rho/\mu}$ can be made arbitrarily small by appropriately selecting the design parameters.

Further, the following dynamics are obtained from (18) and (44):

$$e_u + \lambda_1\int_0^t e_u\,d\tau = \varepsilon_u,$$
$$\dot{e}_\beta + \lambda_2 e_\beta + \lambda_3\int_0^t e_\beta\,d\tau = \varepsilon_\beta, \tag{45}$$

where ε_u and ε_β are arbitrarily small errors.

To prove that e_u and e_β are UUB, the Lyapunov function is given by

$$V_s = \frac{1}{2}\left(\int_0^t e_u\,d\tau\right)^2 + \frac{1}{2}e_\beta^2. \tag{46}$$

The time derivative of this Lyapunov function along the dynamics in (45) is such that

$$\begin{aligned}\dot{V}_s &= e_u\int_0^t e_u\,d\tau + e_\beta\dot{e}_\beta \\ &= -\lambda_1\left(\int_0^t e_u\,d\tau\right)^2 - \lambda_2 e_\beta^2 + \varepsilon_u\int_0^t e_u\,d\tau \\ &\quad - \lambda_3 e_\beta\int_0^t e_\beta\,d\tau + \varepsilon_\beta e_\beta.\end{aligned} \tag{47}$$

From Young's inequality, the following fact is obtained:

$$\begin{aligned}
&\varepsilon_u \int_0^t e_u \, d\tau \le 0.5\lambda_1 \left(\int_0^t e_u \, d\tau \right)^2 + 0.5\frac{\varepsilon_u^2}{\lambda_1}, \\
&-\lambda_3 e_\beta \int_0^t e_\beta \, d\tau \le \frac{\lambda_2 e_\beta^2}{2} + \frac{\lambda_3}{2\lambda_2} \left(\int_0^t e_\beta \, d\tau \right)^2, \\
&\varepsilon_\beta e_\beta \le 0.25\lambda_2 e_\beta^2 + \frac{\varepsilon_\beta^2}{\lambda_2}.
\end{aligned} \tag{48}$$

Then

$$\begin{aligned}
\dot{V}_s \le &-0.5\lambda_1 \left(\int_0^t e_u \, d\tau \right)^2 - 0.25\lambda_2 e_\beta^2 + 0.5\frac{\varepsilon_u^2}{\lambda_1} \\
&+ 0.5\frac{\lambda_3}{\lambda_2} \left(\int_0^t e_\beta \, d\tau \right)^2 + \frac{\varepsilon_\beta^2}{\lambda_2} = -2\mu_s V_s + \rho_s,
\end{aligned} \tag{49}$$

where

$$\begin{aligned}
\mu_s &= \min\left\{0.5\lambda_1, 0.25\lambda_2\right\}, \\
\rho_s &= 0.5\frac{\varepsilon_u^2}{\lambda_1} + 0.5\frac{\lambda_3}{\lambda_2} \left(\int_0^t e_\beta \, d\tau \right)^2 + \frac{\varepsilon_\beta^2}{\lambda_2}.
\end{aligned} \tag{50}$$

Similar to the analysis in (42)~(44), there exists $T_s > 0$ such that, for all $t > T_s$,

$$\left\| \chi_s \right\| \le \sqrt{\frac{\rho_s}{\mu_s}}, \tag{51}$$

where $\chi_s = \{\int_0^t e_u \, d\tau, e_\beta\}$.

It is obvious that $\int_0^t e_u \, d\tau$ and e_β are UUB and will be arbitrarily small by choosing suitable parameters.

From $s_u = e_u + \lambda_1 \int_0^t e_u \, d\tau$, we know e_u will be arbitrarily small. From (6) and (15), we have

$$\begin{bmatrix} u - u_d \\ u\tan\beta - u_d \tan\beta_d \end{bmatrix} = \overline{R} \begin{bmatrix} \dot{x}_e + k_x \left| x_e \right| \operatorname{sign}\left(x_e\right) \\ \dot{y}_e + k_y \left| y_e \right| \operatorname{sign}\left(y_e\right) \end{bmatrix}, \tag{52}$$

where

$$\overline{R} = \begin{bmatrix} \cos\psi & \sin\psi \\ -\sin\psi & \cos\psi \end{bmatrix}. \tag{53}$$

It is clear that $|\overline{R}| = 1$ which indicates that it is nonsingular. Then we have

$$\begin{aligned}
\dot{x}_e &= -k_x \left| x_e \right| \operatorname{sign}\left(x_e\right) + \varepsilon_{xb}, \\
\dot{y}_e &= -k_y \left| y_e \right| \operatorname{sign}\left(y_e\right) + \varepsilon_{yb},
\end{aligned} \tag{54}$$

where ε_{xb}, ε_{yb} are arbitrarily small errors.

Furthermore, consider the following Lyapunov function candidate:

$$V_p = \frac{1}{2}x_e^2 + \frac{1}{2}y_e^2. \tag{55}$$

The time derivative of V_p along the dynamics in (54) is such that

$$\begin{aligned}
\dot{V}_p &= x_e \dot{x}_e + y_e \dot{y}_e \\
&= x_e \left(-k_x \left| x_e \right| \operatorname{sign}\left(x_e\right) + \varepsilon_{xb} \right) \\
&\quad + y_e \left(-k_y \left| y_e \right| \operatorname{sign}\left(y_e\right) + \varepsilon_{yb} \right) \\
&= -k_x \left| x_e \right|^2 - k_y \left| y_e \right|^2 + x_e \varepsilon_{xb} + y_e \varepsilon_{yb} \\
&\le -0.5k_x \left| x_e \right|^2 - 0.5k_y \left| y_e \right|^2 + \frac{\varepsilon_{xb}^2}{2k_x} + \frac{\varepsilon_{yb}^2}{2k_y} \\
&= -2\mu_p V_p + \rho_p,
\end{aligned} \tag{56}$$

where

$$\begin{aligned}
\mu_p &= \min\left\{0.5k_x, 0.5k_y\right\}, \\
\rho_p &= \frac{\varepsilon_{xb}^2}{2k_x} + \frac{\varepsilon_{yb}^2}{2k_y}.
\end{aligned} \tag{57}$$

Also similar to the analysis in (42)~(44), there exists $T_p > 0$ such that, for all $t > T_p$,

$$\left\| \chi_p \right\| \le \sqrt{\frac{\rho_p}{\mu_p}}, \tag{58}$$

where $\chi_p = \{x_e, y_e\}$.

From the reason that ε_{xb} and ε_{yb} are arbitrarily small errors, we know that x_e and y_e are UUB and will be arbitrarily small.

Also, u is continuously differentiable in the moving process of hovercraft. Hence, $\dot{u}$ is bounded. From (6), we have

$$\dot{u} = ur\tan\left(\beta\right) + \frac{R_u + \tau_u}{m}. \tag{59}$$

From (15), Remark 4, and the boundedness of x_e and y_e, we have that u_d and β_d are bounded. Then u, v, and β are bounded from (5) and (17). Furthermore, R_u is bounded from (3). Therefore, it can be concluded that r will remain bounded from (7) and (59). This concludes the proof. □

Remark 6. In order to avoid the well-known chattering problem, the sign function used in the control laws (26) and (27) can be replaced by hyperbolic tangent function which is continuous such that $\operatorname{sign}(s) = \tanh(k_H s)$, where k_H is a positive scalar which can be chosen to get a very good approximation.

4. Simulations

Two different cases are implemented to verify the effectiveness and superiority of the proposed controller. In simulations, the main particulars and constraints of hovercraft are shown in Tables 1 and 2. The water surface is calm without waves.

Table 1: Main particulars of hovercraft.

m (kg)	40000
J_z (kgm^2)	1.8×10^6
S_{PP} (m^2)	45
S_{LP} (m^2)	93
S_{HP} (m^2)	260
Q (m^3/s)	140.8
V_w (knots)	10
l_{sk} (m)	65
B_c (m)	8.9
l_c (m)	23.6
h (m)	1
H_{hov} (m)	5.9
S_c (m^2)	212
β_w (deg)	45

Table 2: State and input constraints.

Variable	Maximum	Minimum
u (knots)	40	25
β (deg)	8	−8
τ_u (N)	80000	−80000
τ_r (Nm)	1×10^5	-1×10^5

The comparisons of three different methods are carried out in each case. The legend "Method A" means the method in [14]; the legend "Method B" means the method without state and input saturation constraints.

Saturation coefficients are

$$\begin{aligned} k_{su} &= 1.2, \\ k_{wu1} &= 1, \\ k_{wu2} &= 903000, \\ k_{\xi u1} &= 31, \\ k_{sr} &= 1.2, \\ k_{wr1} &= 1, \\ k_{wr2} &= 650300, \\ k_{\xi r1} &= 38, \\ k_{\xi u2} &= 0.08, \\ k_{\xi r2} &= 0.08, \\ \overline{\sigma} &= 3, \\ \sigma &= 1. \end{aligned} \tag{60}$$

Case 1. The reference trajectory parameters are

$$\begin{aligned} x_d(0) &= 300\ \mathrm{m}, \\ y_d(0) &= 100\ \mathrm{m}, \\ \psi_d(0) &= 45^\circ, \\ u_{d\mathrm{set}}(t) &= 35\ \text{knots}, \\ v_{d\mathrm{set}}(t) &= 0, \\ r_{d\mathrm{set}}(t) &= 0. \end{aligned} \tag{61}$$

The initial values of hovercraft model are

$$\begin{aligned} x(0) &= 0, \\ y(0) &= 0, \\ \psi(0) &= 70^\circ, \\ u(0) &= 35\ \text{knots}, \\ \beta(0) &= 0, \\ r(0) &= 0. \end{aligned} \tag{62}$$

The controller parameters are

$$\begin{aligned} k_x &= 0.6, \\ k_y &= 0.6, \\ k_1 &= 1.1, \\ \eta_1 &= 0.25, \\ \lambda_1 &= 2, \\ k_2 &= 1.2, \\ \eta_2 &= 0.5, \\ \lambda_2 &= 30, \\ \lambda_3 &= 6, \\ \varepsilon_N &= 0.5. \end{aligned} \tag{63}$$

It is observed from Figures 3–8 that the proposed trajectory tracking controller is effective. Tracking errors of all three methods converge to arbitrarily small values and heading angle is bounded. From the comparisons with Methods A and B in Figures 9 and 10, the proposed controller can limit the surge speed and the drift angle into the safe range effectively. Figures 11 and 12 show that the input saturation is also handled by the proposed controller.

Case 2. The reference trajectory parameters are

$$\begin{aligned} x_d(0) &= -200\ \mathrm{m}, \\ y_d(0) &= 50\ \mathrm{m}, \\ \psi_d(0) &= 45^\circ, \\ u_{d\mathrm{set}}(t) &= 35\ \text{knots}, \\ v_{d\mathrm{set}}(t) &= 0, \\ r_{d\mathrm{set}}(t) &= 0.1^\circ/\mathrm{s}. \end{aligned} \tag{64}$$

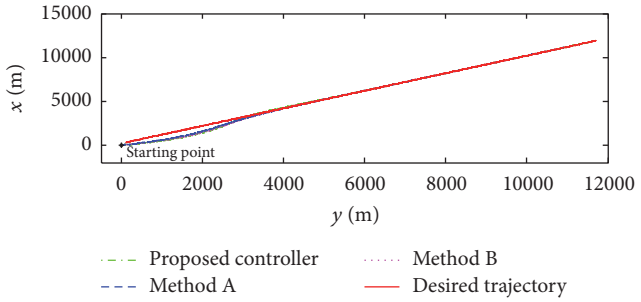

Figure 3: The actual and desired trajectory of hovercraft.

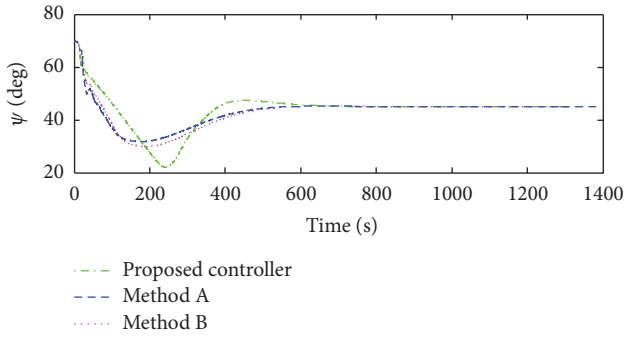

Figure 4: The heading angle of hovercraft.

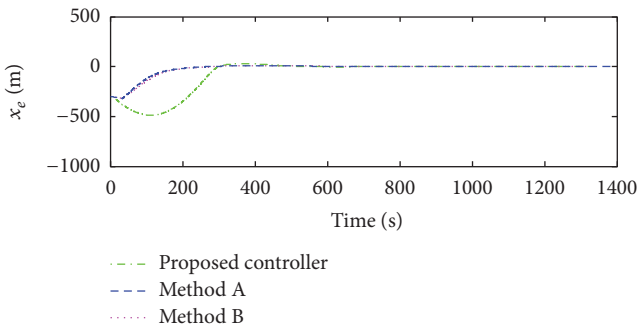

Figure 5: The surge position tracking error.

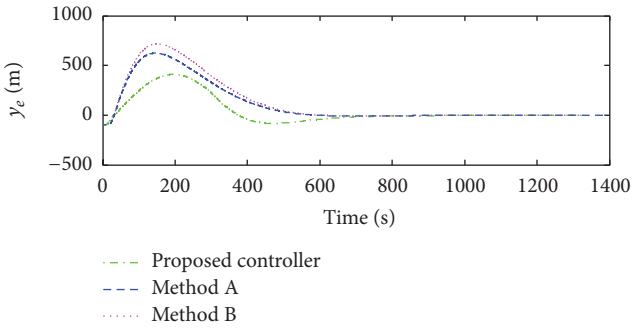

Figure 6: The sway position tracking error.

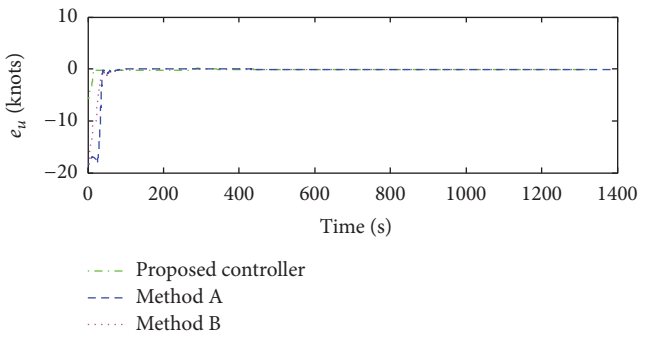

Figure 7: The surge velocity tracking error.

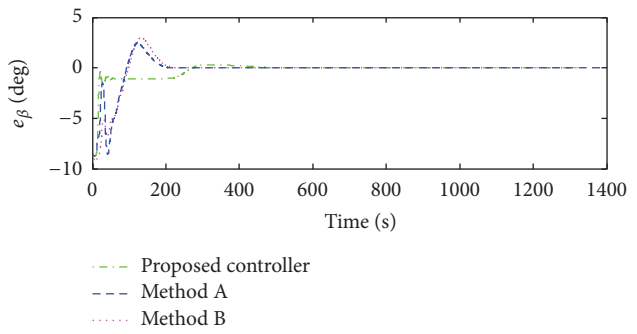

Figure 8: The drift angle tracking error.

The initial values of hovercraft model are

$$\begin{aligned} x(0) &= 0, \\ y(0) &= 0, \\ \psi(0) &= 30^{\circ}, \\ u(0) &= 35 \text{ knots}, \\ \beta(0) &= 0, \\ r(0) &= 0. \end{aligned} \tag{65}$$

The controller parameters are

$$\begin{aligned} k_x &= 0.6, \\ k_y &= 0.6, \\ k_1 &= 1.53, \\ \eta_1 &= 0.1, \\ \lambda_1 &= 4, \\ k_2 &= 1.2, \\ \eta_2 &= 0.5, \\ \lambda_2 &= 30, \\ \lambda_3 &= 2, \\ \varepsilon_N &= 0.5. \end{aligned} \tag{66}$$

It is obvious from Figures 14–19 that only the proposed controller can track the trajectory successfully. Figures 20 and 21 show that the surge speed changes to negative values and the drift angle exceeds the safety limit in the tracking control

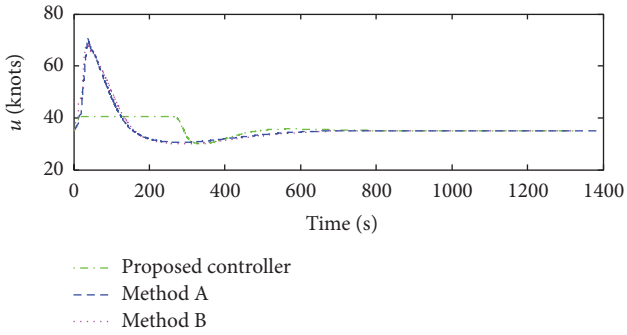

Figure 9: The surge velocity of hovercraft.

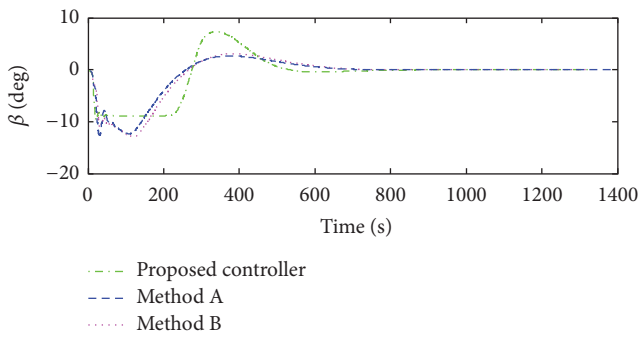

Figure 10: The drift angle of hovercraft.

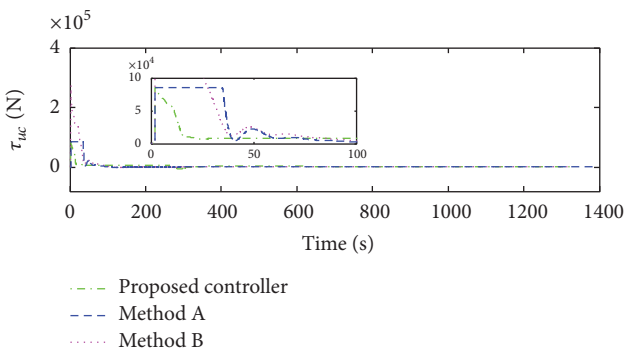

Figure 11: The surge control law of hovercraft.

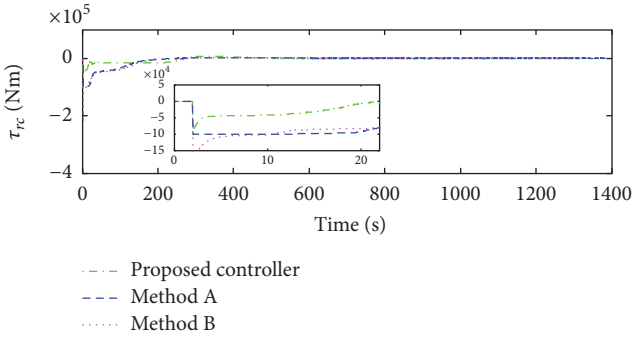

Figure 12: The yaw control law of hovercraft.

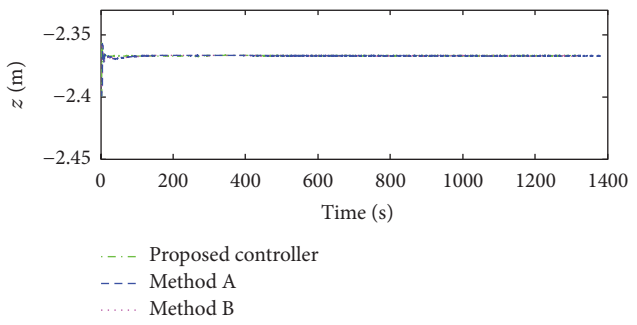

Figure 13: The heave position of hovercraft.

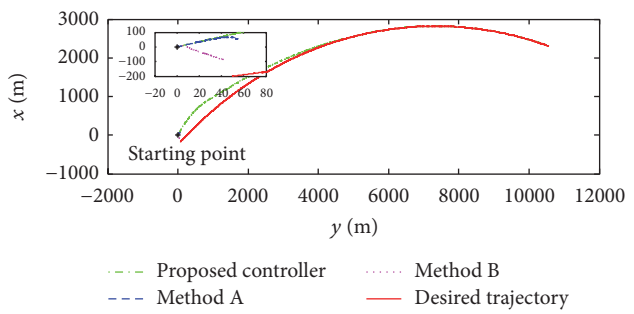

Figure 14: The actual and desired trajectory of hovercraft.

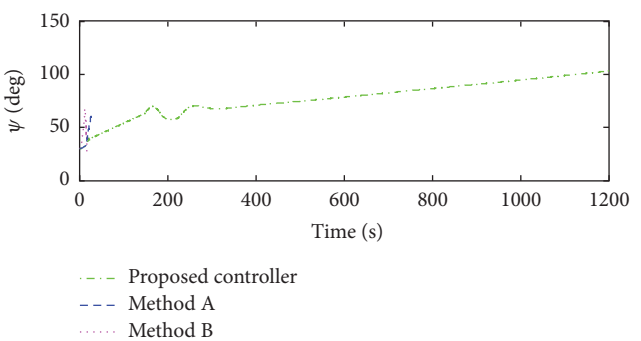

Figure 15: The heading angle of hovercraft.

process of Methods A and B. These are absolutely not allowed for hovercraft. In contrast, you can see from Figure 20 that surge speed can still be positive, even large enough to avoid the influence of the resistance humps under the control of the proposed controller. And drift angle is also within the safety limit from Figure 21. From Figures 22 and 23, we know that the input constraint ability of the proposed controller is effective. Figures 13 and 24 show the heave position of hovercraft.

5. Conclusion

A safety-guaranteed trajectory tracking controller has been proposed for underactuated hovercraft in this paper. The safety-guaranteed auxiliary dynamic system is designed to deal with state and input constraints. The velocity of hovercraft is constrained to eliminate the effect of resistance hump and obtain better stability. The safety limit of drift angle is carried out effectively for safety in the high-speed trajectory tracking process of hovercraft. The input saturation is handled. High nonlinearity and model uncertainties are approximated by RBFNNs. Simulation results have been

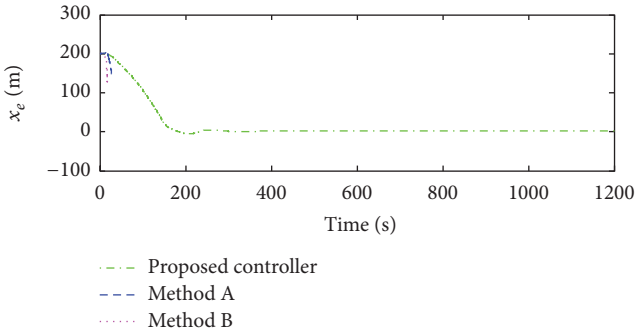

Figure 16: The surge position tracking error.

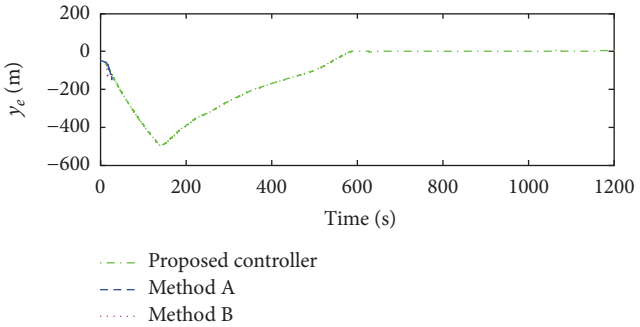

Figure 17: The sway position tracking error.

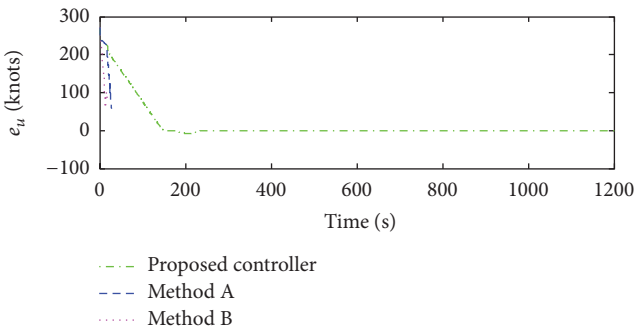

Figure 18: The surge velocity tracking error of hovercraft.

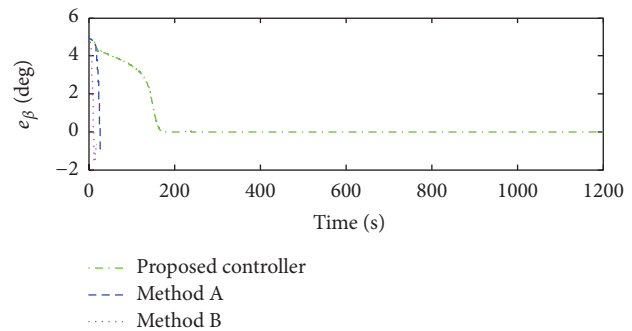

Figure 19: The drift angle tracking error of hovercraft.

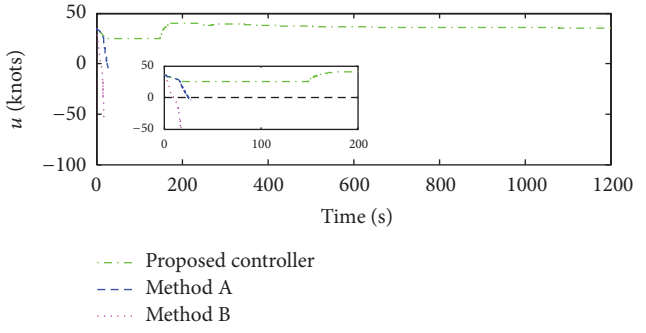

Figure 20: The surge velocity of hovercraft.

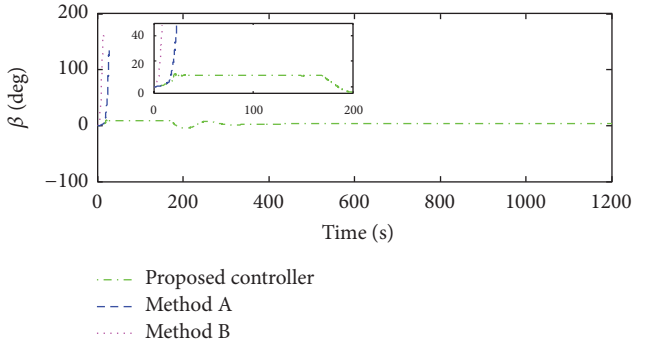

Figure 21: The drift angle of hovercraft.

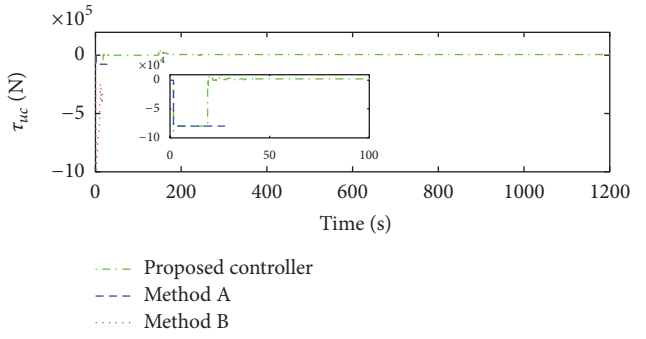

Figure 22: The surge control law of hovercraft.

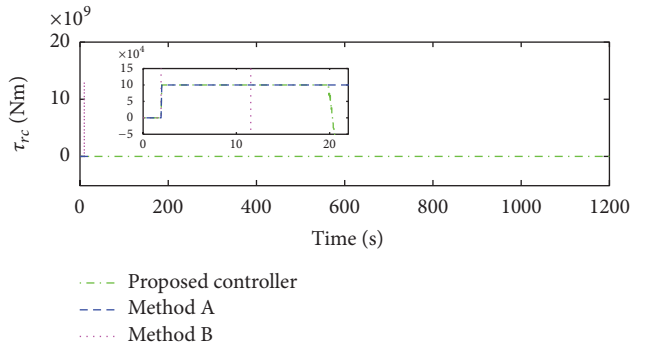

Figure 23: The yaw control law of hovercraft.

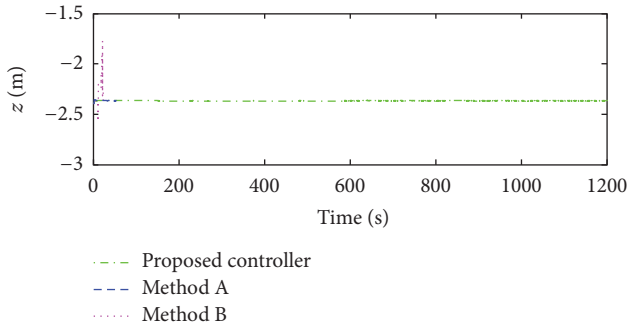

Figure 24: The heave position of hovercraft.

presented to illustrate the effectiveness of the proposed controller.

Conflicts of Interest

The authors declare that there are no conflicts of interest regarding the publication of this paper.

Acknowledgments

The supports of the National Natural Science Foundation of China (Grant no. 51309062) and the project "Research on Maneuverability of High Speed Hovercraft" (Project no. 2007DFR80320) are gratefully acknowledged.

References

[1] Y. Liang and A. Bliault, *Theory & Design of Air Cushion Craft*, Arnold, 2000.

[2] H. Sira-Ramírez, "Dynamic second-order sliding mode control of the hovercraft vessel," *IEEE Transactions on Control Systems Technology*, vol. 10, no. 6, pp. 860–865, 2002.

[3] J. Aranda, "A Control for tracki-ng and stabilization of an under-actuated nonlinear RC hovercraft," *International Federation of Auto-matic Control*, 2006.

[4] J. Zhao and J. Pang, "Trajectory control of underactuated hovercraft," in *Proceedings of the 2010 8th World Congress on Intelligent Control and Automation (WCICA '10)*, pp. 3904–3907, July 2010.

[5] R. Morales, H. Sira-Ramírez, and J. A. Somolinos, "Linear active disturbance rejection control of the hovercraft vessel model," *Ocean Engineering*, vol. 96, pp. 100–108, 2015.

[6] G. G. Rigatos and G. V. Raffo, "Input–output linearizing control of the underactuated hovercraft using the derivative-free nonlinear kalman filter," *Unmanned Systems*, vol. 03, no. 02, pp. 127–142, 2015.

[7] K. Shojaei, "Trajectory tracking control of autonomous underactuated hovercraft vehicles with limited torque," in *Proceedings of the 2014 2nd RSI/ISM International Conference on Robotics and Mechatronics (ICRoM '14)*, pp. 468–473, October 2014.

[8] K. Shojaei, "Neural adaptive robust control of underactuated marine surface vehicles with input saturation," *Applied Ocean Research*, vol. 53, pp. 267–278, 2015.

[9] M. Cohen, T. Miloh, and G. Zilman, "Wave resistance of a hovercraft moving in water with nonrigid bottom," *Ocean Engineering*, vol. 28, no. 11, pp. 1461–1478, 2001.

[10] Y. Yang, Z. K. Zhang, and M. D. Amp, "iscussion and practice about hump transition problem of high-density air medium-low speed ACV," *Ship & Boat*, 2014.

[11] H. Fu, "Analysis and consider- ation on safety of all-lift hovercraft," *Ship & Boat*, 2008.

[12] M. Tao and W. Chengjie, *Hovercraft performance and skirt-cushion system dynamics design*, National Defence Industry Press, 2012.

[13] G. Zilman, "Mathematical simula- tion of hovercraft maneuverin- g," *Proceedings of the Twenty-Third American Towing tank Conference*, pp. 373–382, 1993.

[14] J. Du, X. Hu, M. Krstić, and Y. Sun, "Robust dynamic positioning of ships with disturbances under input saturation," *Automatica*, vol. 73, pp. 207–214, 2016.

[15] M. Chen, S. S. Ge, and B. Ren, "Adaptive tracking control of uncertain MIMO nonlinear systems with input constraints," *Automatica*, vol. 47, no. 3, pp. 452–465, 2011.

[16] S. Li, Y. Wang, J. Tan, and Y. Zheng, "Adaptive RBFNNs/integral sliding mode control for a quadrotor aircraft," *Neurocomputing*, vol. 216, pp. 126–134, 2016.

[17] K. Xia and W. Huo, "Robust adaptive backstepping neural networks control for spacecraft rendezvous and docking with input saturation," *ISA Transactions*, vol. 62, pp. 249–257, 2016.

[18] J. Feng and G.-X. Wen, "Adaptive NN consensus tracking control of a class of nonlinear multi-agent systems," *Neurocomputing*, vol. 151, no. 1, pp. 288–295, 2015.

[19] T. Elmokadem, M. Zribi, and K. Youcef-Toumi, "Trajectory tracking sliding mode control of underactuated AUVs," *Nonlinear Dynamics*, vol. 84, no. 2, pp. 1079–1091, 2016.

[20] T. Elmokadem, M. Zribi, and K. Youcef-Toumi, "Terminal sliding mode control for the trajectory tracking of underactuated Autonomous Underwater Vehicles," *Ocean Engineering*, vol. 129, pp. 613–625, 2017.

[21] V. K. Dyachenko, *Resistance of Air Cushion Vehicle*, Central Research Institute of ACAD, Krylov, 1999.

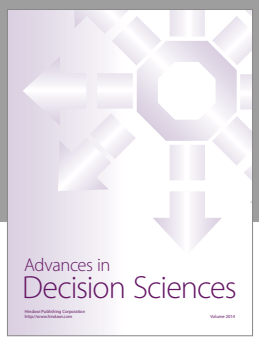

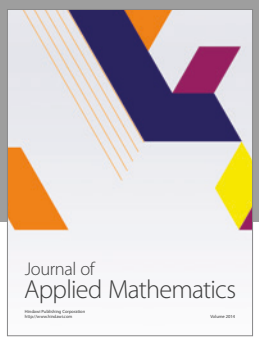

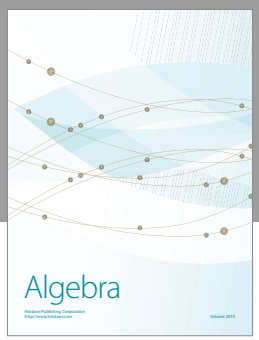

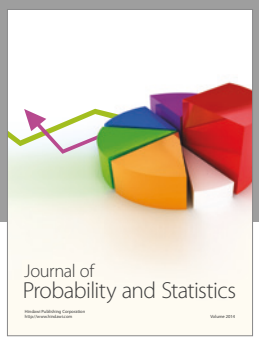

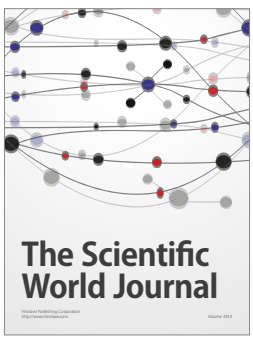

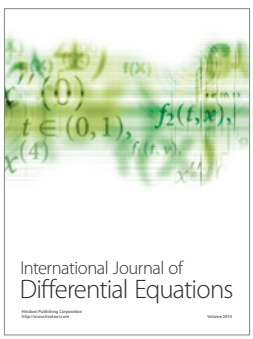

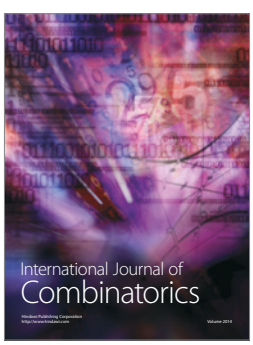

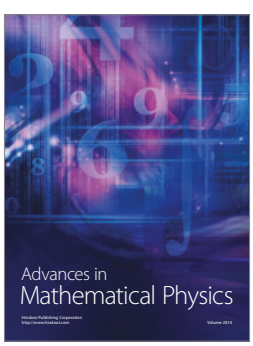

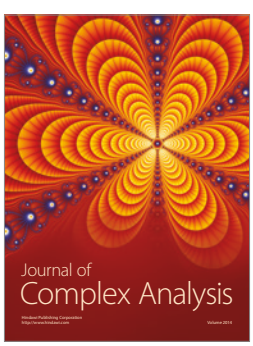

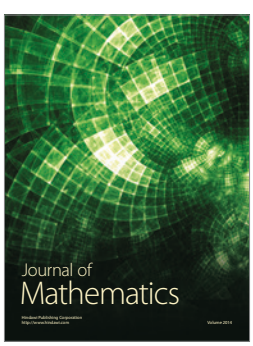

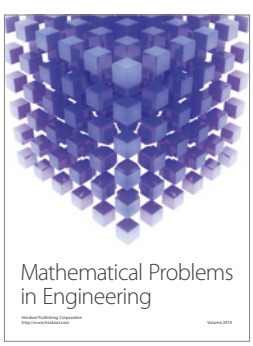

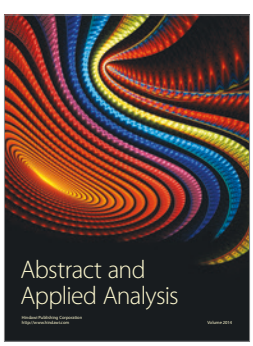

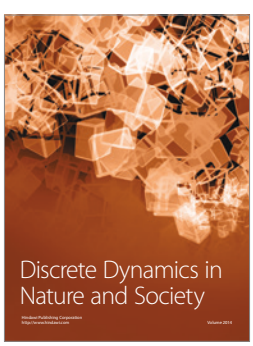

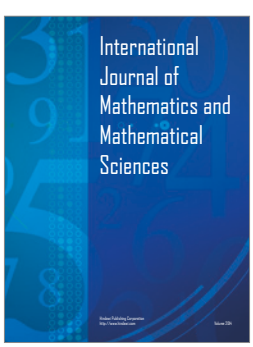

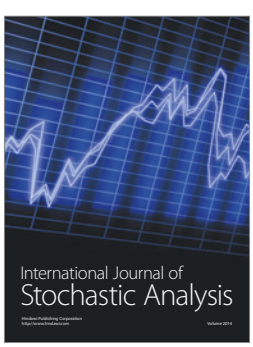

Hindawi

Submit your manuscripts at
https://www.hindawi.com